ADVANCED FUNCTIONAL MATERIALS
www.afm-journal.de

The Cribellate Nanofibrils of the Southern House Spider: Extremely Thin Natural Silks with Outstanding Extensibility

*Jacob Silliman, Sean R. Koebley, and Hannes C. Schniepp**

Cribellate silks, produced by ancient spiders, are fascinating because they feature a highly sophisticated, 3D hierarchical structure consisting of filaments with different diameters and shapes. Here, the smallest and thinnest constituents of the cribellate silk are investigated: nanofibrils that form a dense mesh that is supported by larger fibers. Analysis of their structure via atomic force and transmission electron microscopies shows that they are flattened fibrils, only ≈5 nm thick — thinner than any other natural spider silk fibrils previously reported. In this work, the first mechanical tensile testing experiments on these fibrils are carried out, which reveals that the fibrils show an outstanding extensibility of at least 1100%, almost twice as much as the most stretchable spider silk previously reported. Based on these extraordinary findings, this work significantly expands the parameter space of materials properties attainable by spider silks and provides further insights into their nanomechanics.

1. Introduction

Spider silk is widely recognized as a prototype for a biocompatible, sustainable polymer with outstanding mechanical properties.[1–3] Its specific strength is impressive and outperforms steel by a factor of ≈5. However, where it truly stands out is in its combination of high strength with unusually high extensibility, which makes silk one of the toughest known materials.[4] Nanofibrils have long been recognized as an important element in silks,[5] but only recently, a picture has been emerging according to which silks virtually exclusively consist of uniform and axially aligned nanofibrils,[6,7] with relatively weak inter-fibrillar forces.[6,8] Therefore, the extraordinary mechanical properties of spider silk have to have their origin in the nanofibrils, which makes their study a high priority.[8,9] Direct characterization of individual silk nanofibrils is a desirable goal; however, in most cases, nanofibrils are part of a bundle of thousands of nanofibrils to form a much thicker fiber.[10–12] Preparation of individual nanofibrils has been accomplished via mechanical or chemical exfoliation procedures. The problem with these methods, however, is that they are invasive and bear a risk of altering the mechanical or chemical properties of the nanofibrils. Here we study the cribellate silk of the southern house spider *Kukulkania hibernalis* (*K. hibernalis*), which contains thousands of individual nanofibrils that are similar in size and shape to the nanofibrils constituting larger silk fibers. We exploit this opportunity to characterize their structure and, for the first time, their mechanical properties directly.

A few natural silk fibrils with sub-100 nm dimensions have been looked at more closely in the literature. The webspinner insects (embiids) spin silk fibers as small as 65 nm in diameter,[13–15] spider mite silk is cylindrical with a diameter of ≈50 nm,[16] and the ribbon-like silk of the recluse genus of spiders (*Loxosceles*) is ≈50–80 nm thick.[17–19] Cribellate silk is a particularly interesting example of a nanoscale silk, produced by some of the most ancient spider species.[20,21] This silk is a hierarchical composite of larger reinforcing strands and a nanofibrillar mesh. The nanofibrils were previously reported as 20–100 nm in diameter[22,23] and are extruded from the cribellum—a plate on the rear of the abdomen containing hundreds of tiny nozzles—before being combed into a mesh by the spider's rear legs.[22,24,25] In contrast to the more well-known orb-web silks, in which prey is captured by regularly spaced glue droplets,[3,26] a cribellate strand ensnares prey in the capture mesh via entanglement, van der Waals forces, and capillary adhesion.[27,28] Here, we investigate the cribellate nanofibrils of the southern house spider (*K. hibernalis*). A widespread species in the southern U.S., Central America, and South America, *K. hibernalis* belongs to the most ancient extant family (Filistatidae) within an ancient spider superfamily (Haplogynae), which also contains the *Loxosceles* genus.[29] The mesh fibrils in *K. hibernalis* cribellate silk have been reported to be ribbon-like,[22,30,31] although there is not a full consensus in the literature on this issue, since one source actually reported these nanofibrils to be of cylindrical morphology.[32]

Characterizing the mechanical properties of silk fibers becomes increasingly challenging for smaller and smaller fibrils. The elastic modulus of several cribellate spiders was characterized using peak-force tapping atomic force microscopy (AFM).[33]

J. Silliman, S. R. Koebley, H. C. Schniepp
Department of Applied Science
William & Mary
P.O. Box 8795, Williamsburg, VA 23187, USA
E-mail: schniepp@wm.edu

The ORCID identification number(s) for the author(s) of this article can be found under https://doi.org/10.1002/adfm.202408409

DOI: 10.1002/adfm.202408409

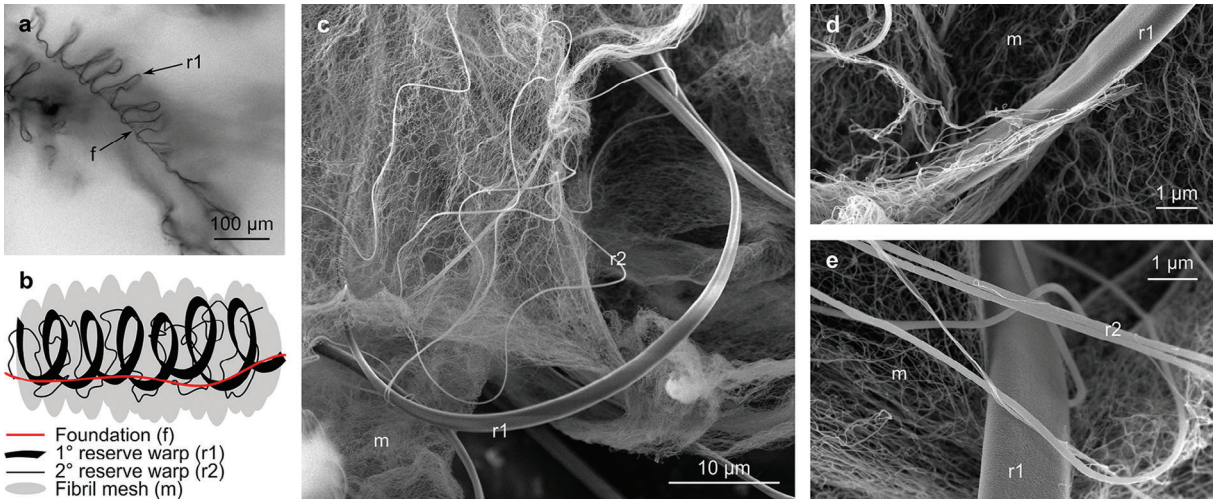

Figure 1. The cribellate capture strand of *K. hibernalis*. a) Optical image of the cribellate composite. The primary reserve warp (r1) forms helical loops around the central foundation fiber (f). b) Schematic of the cribellate strand. c–e) SEM images displaying the flattened primary reserve warp (r1), cylindrical secondary reserve warp (r2), and fibril mesh (m) components of a capture thread.

This technique, in essence, compresses the fibrils on a substrate of known stiffness, which can be used to determine the elastic modulus of silks[34] with some limitations in accuracy. However, since the really outstanding properties of silk are its strength, extensibility, and toughness, the most interesting aspects of silk require exploring its high-strain regime, which cannot be accomplished by peak-force tapping AFM or optical techniques,[35] which only test low strains. Traditional tensile testing is challenging for nanofibrils, due to difficulties in sample preparation, limited force sensitivity, and transducer accuracy. AFM-based three-point deformation experiments yield consistent and reliable results for nanoscale objects suspended across a gap[36] and have successfully been used for carbon nanotubes,[37] cellulose nanofibrils,[38] and spider mite silk nanofibrils.[16] However, in all of these cases, the degree of bending was not large, and the measurements were limited to determining Young's modulus. The measurements on spider mite silk, which is an order of magnitude larger than the *K. hibernalis* cribellate nanosilks, found Young's modulus of ≈24 GPa,[40] similar to *T. clavipes*.[39] True tensile tests on sub-100 nm single spider silk nanofibrils have, to the best of our knowledge, not previously been achieved.

For this work, we first conducted imaging of *K. hibernalis* nanofibrils via high-resolution AFM, as well as scanning and transmission electron microscopies (SEM and TEM) to gain new insights on their nanostructure. We found that they were thinner than any silk previously reported. We then carried out three-point deformation tests of these nanofibrils suspended across 200 nm-diameter holes. Our bending tests went deep enough for the nanofibrils to reach strains in excess of 1000%, much higher than what had previously been demonstrated for any spider silk.

2. Results and Discussion

2.1. Morphology of the Cribellate Silk and Nanofibrils

Our optical microscopy and SEM evidence of *K. hibernalis* cribellate silk showed its typical composite structure, featuring a mesh of fibrils anchored by three types of reinforcing fibers (**Figure 1**). The foundational fiber (f) serves as the guiding backbone to support the capture mesh; the larger, primary reserve warps (r1's) feature a flattened morphology and are helically arranged; the secondary reserve warps (r2's) are cylindrical and dispersed throughout the mesh; the even smaller cribellate fibrils are interweaving to form the mesh.[22]

The fibrils comprising the cribellate mesh were imaged by SEM, TEM, and AFM (**Figure 2**). The TEM images indicated a ribbon-like morphology of the fibrils with an average width of ≈38 nm; the fibrils were observed to roll up into themselves, adhere to one another at junctions, and combine to form wider, overlapping ribbons (Figure 2a–d). The AFM results further corroborated the ribbon-like morphology of the nanofibrils, showing an average thickness of 5.1 ± 0.9 nm and a width of 30.2 ± 7.8 nm ($n = 27$). In some cases, they showed a tendency to split into two sub-fibrils (Figure 2e). Quantitative dimensional assessments via AFM can be inaccurate; widths tend to be overestimated due to probe convolution effects; heights measured via dynamic-mode imaging can be underestimated for other reasons.[40] However, since we measured heights via contact-mode imaging, and since we found agreement between TEM and AFM images, we consider the ribbon-like nature of the nanofibrils confirmed, which settles the previously mentioned controversy in the literature. Furthermore, the fibril surfaces featured protruding nodes of unknown nature in both TEM (Figure 2c) and AFM (Figure 2e–f).

At 5 nm thick and 30–40 nm wide, a *Kukulcania* fibril is the smallest silk ever measured; compared to the 65 nm-diameter embiid silks or 20–100 nm-diameter cylindrical cribellate fibrils, *K. hibernalis* fibrils are clearly thinner.[13,15,33,41] The splitting of a fibril into two sub-fibrils is particularly interesting, as the 10–20 nm-width sub-fibrils (Figure 2f) appear to match the dimensions of the "base fibrils" observed in several other studies of native silk[5–7] and artificially assembled silk.[7,42–44] One possibility is that the ribbon shape of this silk simply comes

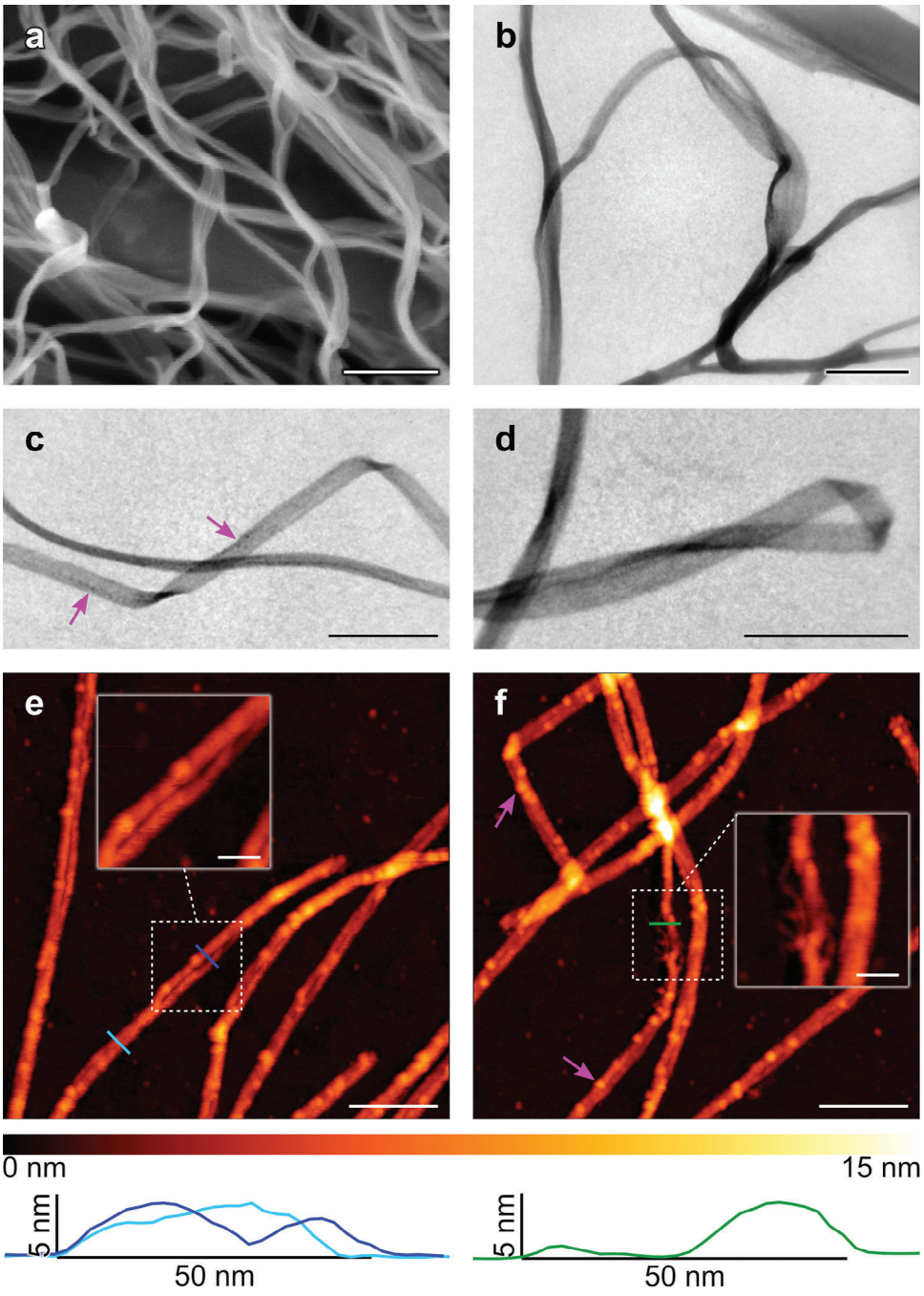

Figure 2. Fibrils comprising the *K. hibernalis* cribellate mesh. a) SEM image of fibrils adhered and looped with one another to form the cribellate mesh. b) TEM image of fibrils rolled up into themselves and one another. c,d) TEM of ribbon-like fibrils, with occasional darker areas of greater density (purple arrows). e) Contact mode AFM scans indicate a fibril height of 5 nm and width of ≈45 nm (cyan cross-section). In several areas, a fibril splits into two cylindrical cords (inset, blue cross-section). f) AFM scan of fibrils, with visible protrusions (purple arrows).

from several nanofibril running parallel in a "flat" (single-layer) configuration.

This study and many others suggest that these "base fibrils" are the fundamental modules of mesoscale fibril assembly. Thus, *K. hibernalis* fibrils offer the closest natural approximation of the base unit of silk assembly, allowing the fundamentals of silk structure and formation to be studied.

2.2. Mechanical Characterization of Cribellate Nanofibrils

We exploited the availability of individual nanofibrils in the cribellate silk of *K. hibernalis* to characterize the mechanical properties of these extremely thin strands via AFM (see schematic in **Figure 3**a). Therefore, we deployed this silk on silicon nitride (Si_3N_4) substrates featuring a hexagonal pattern of

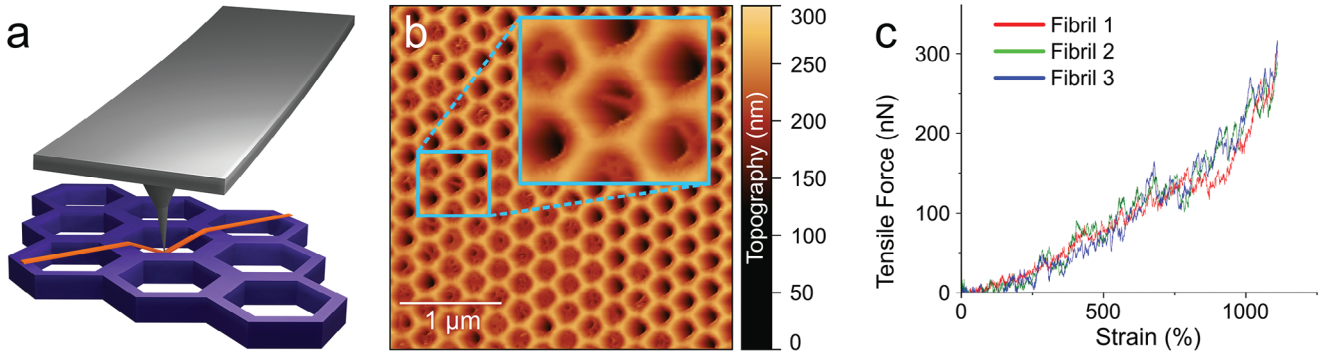

Figure 3. AFM-based mechanical testing of *K. hibernalis* cribellate nanofibrils. a) Schematic of three-point deformation testing. b) AFM image of fibrils placed on top of a Si_3N_4 substrate featuring a hexagonal array of 200 nm-diameter holes. Inset: close-up of a nanofibril, suspended across the center of a hole. c) Force curves taken on 3 nanofibrils produced very similar results, indicating that our experiments reflect the intrinsic mechanical behavior of *K. hibernalis* nanofibrils.

200 nm-diameter holes. Figure 3b shows a tapping-mode AFM image of the Si_3N_4 substrate; silk fibrils can be seen in several locations (see inset). We selected locations in which individual, small silk fibrils ran straight across a hole, close to the hole's center. By conventional standards of AFM imaging, this type of sample represents a significant challenge, because there are very large and very sudden topography changes between the top of the substrate level and the inside of the holes that are microns deep. With the extremely thin nanofibrils suspended across these holes, intuition might suggest that these nanofibrils would be easily ruptured or displaced under these extreme imaging conditions. Nevertheless, the observed imaging conditions were very stable; suspended nanofibrils could routinely be imaged, without evidence of fibril rupture, distortion, relocation, or disappearance. These observations indicate that the fibrils are surprisingly robust and that they are attached to the substrate relatively strongly. Subsequently, we placed the same tapping-mode AFM probe directly above the suspended fiber, at the midpoint of the suspended region. From that point, we performed several vertical force-versus-displacement experiments, as commonly done in force spectroscopy, at a regular humidity level of 47 ± 5%. Accordingly, the AFM probe was lowered at constant velocity to first land on the suspended nanofibril and then move downward farther, to increasingly deform the suspended nanofibril while recording the cantilever deflection.

The onset of the fibril deformation caused by vertical AFM probe movement is, in essence, a three-point bending test, where double-clamped boundary conditions apply due to the extreme thinness of the fibrils.[36] When vertical fibril deformation, h, exceeds the fibril radius, R, stretching of the fibril needs to be considered in addition to bending. The contribution from bending becomes insignificant at deep indentations where z surpasses πR. Very deep indentations, more than an order of magnitude greater than πR, were reached during our tests. Therefore, the bending regime is ignored in the interpretation of the acquired force curves, and our experiments can be viewed as essentially tensile tests. The vertical force-versus-deformation data can readily be converted into tensile force-versus-strain within the fibril.[17] This analysis is described in the methods section under "*Data Processing of Mechanical AFM Data*" with more details in Section S2 (Supporting Information), with supporting Figure S2 (Supporting Information).

A representative set of the obtained tensile force-versus-strain data from this experiment after the conversion is shown in Figure 3c. One major surprise from this data is that the *K. hibernalis* nanofibrils were able to sustain extremely large strains and were ultimately stretched to many times their original length without rupturing. Regular AFM probes featuring tip angles of ≈40° were only able to go 300 nm deep into the 200 nm-diameter holes before hitting the side walls. (See Section S1, Figure S1, Supporting Information.) The maximal strain achievable under these conditions was 250%, which did not bring any of the nanofibrils to failure. Consequently, we used high-aspect ratio AFM probes with a small opening angle of <5°, which allowed us to probe anywhere from 1.5 μm to 3 μm deep into the 200 nm-diameter holes in the substrate. (See characterization details in Section S3, Figure S3, Supporting Information.) Even in this case, we did not observe nanofibril rupture; the tested fibrils were able to sustain an average strain of ≈1100%.

We found it somewhat surprising that it was possible to land a relatively sharp AFM probe on a single nanofibril and then stretch this nanofibril to several times its original length by pushing down. Instead, it might seem possible or likely that the AFM probe would slip and subsequently slide past the nanofibril. In this case, a sudden or discontinuous event would likely be observed in the force curve. However, we did not observe any such events in our force data. Another concern was that the nanofibrils slipped on the substrate during the experiment, as the stress level in the fibrils built up. In this case, more and more fibril material would have moved into the 200 nm-diameter hole area to relax the suspended nanofibril. However, we were able to demonstrate that the fibril deformation induced by our AFM indentation experiments was largely elastic. Considering not only indentation but also the corresponding relaxation curves, we saw that the behavior was near-elastic (see Figure S4, Supporting Information). Even when we repeated a force curve three times at the same position of the sample (same nanofibril), the onset of the force sensed by the AFM probe was consistently at the same vertical position. Slip, on the other hand, would permanently move the point of force onset toward deeper indentation.

We were able to acquire valid force curves from three different suspended nanofibrils using two different AFM probes, and all three curves are in good agreement (Figure 3c). This suggests that all curves were taken from fibrils of near-identical thicknesses or cross-sectional areas. Therefore, the likelihood is high that all curves were from single *K. hibernalis* nanofibrils. Due to the very high corrugation and topography of the Si_3N_4 substrates, we were unable to determine the topography profiles of the nanofibrils investigated to directly confirm this, which will be addressed in future work. In the absence of the ability to determine precise cross-sectional areas, we are unable to make quantitative determinations regarding the silk's elastic modulus, strength, or toughness. However, assuming a rough estimate of fibril cross-sectional areas on the order of 150 nm^2 based on AFM images acquired on flat substrates (see cross-sections in Figure 2), the fibrils feature strengths on the order of at least 1 GPa, comparable to other spider silks.

The extremely high nanofibril strains observed, in excess of 1000%, were unexpected; this behavior has not been observed for any type of silk fiber. The largest previously reported breaking strain for silk fibers was 300% for the viscid silk of the *A. diadematus*.[45] Our observations are significantly larger; however, this is in line with what has been observed for many nanomaterials that their mechanical performance, including strain at break, is much higher than for their macroscopic counterparts.[46] The differences are usually due to imperfections and stress concentration in larger specimens. Nanoscopic materials are typically not affected by such imperfections; they exhibit behavior that is more directly in line with the molecular properties of the materials. Therefore, the direct study of the mechanical properties of spider silk nanofibrils has the potential to provide deep insight into their internal mechanics that can be directly related to their molecular structure, which is becoming available with a high degree of detail.[8] The molecular structure of cribellate silk nanofibrils is not yet understood in great detail; however, one study has suggested that it is significantly more amorphous compared to dragline silk,[33] which may be related to the high extensibility we observed. Moreover, it has been shown that proteins in β-helical secondary structure can reach maximum strain values of almost 2000%.[47] Flagelliform silk has a greater number of β-turns, resulting in regions that form β-helices, providing an overall greater extensibility.[48]

3. Conclusion

High-resolution SEM and AFM imaging revealed that the nanofibrils of the *Kukulcania* cribellate silk feature a ribbon morphology, only 5 nm thick and 30 nm wide—the thinnest, smallest natural spider silk fibers reported to date. These flattened fibrils were observed to split into smaller sub-fibrils that matched the dimensions of "base fibrils" reported in other silk studies, which might suggest that the notion of "base fibrils" applies to a large range of different silks, with the *K. hibernalis* being an extreme example where the nanoribbons only consist of about two nanofibrils.

Mechanical testing showed that these extremely thin cribellate nanofibers have the highest extensibility of any silk studied thus far, at least 1100%. Without a large surrounding matrix or other nanofibrils and potential stress concentrations, these fibrils may reveal silk's unconstrained mechanical performance, solely limited by its molecular properties. We believe that our new way of studying silk mechanics will further our insight into understanding silks from the molecular level all the way to the macroscale, where the nanoscale mechanical behavior we revealed can be directly related to the protein sequence and protein secondary structure of spider silk. The data that our type of experiment provides can thus also be used to inform improved models of spider silk.

4. Experimental Section

Spider Sourcing and Optical Microscopy: The *K. hibernalis* specimens were housed individually and fed a weekly diet of crickets. Optical imaging was carried out using a Nikon SMZ-800 stereo microscope using a halogen "gooseneck" lamp for illumination.

Transmission Electron Microscopy: Collected *K. hibernalis* silk was applied to a Formvar-coated grid, stained with 2% uranyl acetate and Reynold's lead citrate, and imaged (Zeiss 109 TEM).

Scanning Electron Microscopy: Samples were prepared by collecting silk at native tension from the web, with the silk severed from its moorings with a heated wire. After being applied to carbon tape, the silk was coated with 2–3 nm of Au-Pd and imaged in the SEM at 1.5–5 kV (Hitachi S4700).

Atomic Force Microscopy: AFM silk samples were collected, applied to freshly cleaved mica, and wetted by depositing 20 µL of Millipore water, followed by spin-coating (Laurell, MODEL). Scanning was conducted with an NTegra Scanning Probe Laboratory (NT-MDT) using both contact mode (µMasch, 0.27 N m^{-1} nominal spring constant) and non-contact mode (ACTA, 40 N m^{-1} nominal spring constant). Raw AFM scans were processed using ImageAnalysis (NT-MDT) and Gwyddion (https://gwyddion.net).

Mechanical Three-Point Deformation Testing of Nanofibrils: Samples for AFM-based three-point deformation testing were prepared with fresh *K. hibernalis* silk. Therefore, the spider was removed from its enclosure onto a sterile piece of cloth, where it was allowed to roam, to leave behind a trail of silk.

Two separate methods yielding similar results were used to prepare samples for AFM scanning and force spectroscopy. The first method involved removing the silk from the cloth and depositing it onto a holey SiN TEM grid (Ted Pella PELCO Holey Silicon Nitride Support Film, 200 nm pores). A pipette was used to deposit 10 µL of deionized water onto the sample for spin-coating at 5000 RPM for 1 minute. This was repeated thrice, then the sample was left to vacuum dry overnight. The second method involved removing the silk from the cloth and tip-sonicating it, with a Cole-Parmer EW-04711-40 Homogenizer (750 Watt) in a 50 mL beaker with 20 mL of deionized water at a maximum amplitude of 40% for 40 minutes with a 10 s on/10 s off pulse pattern. This method was gentle enough to separate the cribellate silk from the larger reserve warps and leave behind a solution of suspended cribellate nanofibrils. 10 µL of this solution was then deposited onto a holey SiN TEM grid and left to incubate for 24 h. After incubation, the sample was lyophilized (Labconco Freezone Triad Cascade Benchtop), after being frozen with liquid nitrogen.

Non-contact amplitude-modulation AFM was conducted 72 h later, on all samples, to ensure the nanofibrils had equilibrated to regular ambient humidity (47 ± 5%). A topography map of the sample using high-aspect ratio TESPA-HAR probes (NanoWorld) was obtained. Individual cribellate silk nanofibrils running across the center of one of the 200 nm pores were identified. The instrument was subsequently switched into contact mode, and deflection-versus-displacement curves were collected after landing the probe on the midpoints of the suspended regions of individual cribellate nanofibrils. This was done with three different high-aspect ratio AFM probes on four independently prepared samples, and four separate nanofibrils found on these samples.

Data Processing of Mechanical AFM Data: A series of data transformations was carried out to convert deflection-versus-displacement curves

into tensile force-versus-strain curves for the nanofibrils. First, measurements of the physical cantilever deflection were calibrated for each probe, by acquiring force curves on the hard Si_3N_4 substrate, which allowed the authors to determine the inverse optical lever sensitivity from the constant-compliance region. (Details in Section S3 with supporting Figure S3, Supporting Information.) Spring constants for individual probes were provided by NanoWorld and double-checked using the Sader method, which allowed the authors to convert the curves into (vertical) force-versus-displacement through Hooke's law. For each data point of these curves, the vertical deformation of the suspended nanofibrils was calculated by subtracting the cantilever deflection from the *z* displacement. Finally, the vertical force F_V was converted into a tensile force F_T in the fiber, by projecting the vertical force vector onto the axis of the deformed fibril,

$$F_T = \frac{F_V\sqrt{h^2 + \left(\frac{L_0}{2}\right)^2}}{2h} \quad (1)$$

where h is the vertical indentation, and L_0 is the hole diameter and, therefore, also the original length of the suspended fibril segment (see Figure S2, Supporting Information). Similarly, the vertical deformation of the suspended fibril was converted into nanofibril tensile strain via the application of the Pythagorean theorem,

$$\varepsilon = 2\frac{\sqrt{h^2 + \left(\frac{L_0}{2}\right)^2}}{L_0} - 1 \quad (2)$$

Supporting Information

Supporting Information is available from the Wiley Online Library or from the author.

Acknowledgements

This material is based upon work supported by the National Science Foundation under Award Nos. DMR-1905902, DMR-2105158 and DMR-1352542.

Conflict of Interest

The authors declare no conflict of interest.

Author Contributions

Conceptualization was done by H.C.S. Methodology and mechanical characterization was done by J.S. Validation was done by H.C.S. Formal analysis was done by J.S. Investigation and mechanical characterization was done by J.S. Investigation and structure imaging was done by S.R.K. H.C.S., J.S., and S.R.K. wrote the original draft. H.C.S. and J.S. reviewed and edited the manuscript. Visualization was done by S.R.K., J.S., and H.C.S. Supervision was done by H.C.S. Funding was acquired by H.C.S.

Data Availability Statement

The data that support the findings of this study are openly available in the Harvard Dataverse at https://doi.org/10.7910/DVN/Q05QVG, reference number.[49]

Keywords

biomaterials, mechanical testing, nanofibrils, protein-based materials, spider silks

Received: May 15, 2024
Revised: July 21, 2024
Published online:

[1] F. G. Omenetto, D. L. Kaplan, *Science* **2010**, *329*, 528.
[2] H. Tao, D. L. Kaplan, F. G. Omenetto, *Adv. Mater.* **2012**, *24*, 2824.
[3] F. Vollrath, D. P. Knight, *Nature* **2001**, *410*, 541.
[4] F. K. Ko, J. Jovicic, *Biomacromolecules* **2004**, *5*, 780.
[5] Q. Wang, H. C. Schniepp, *JOM* **2019**, *71*, 1248.
[6] Q. Wang, H. C. Schniepp, *ACS Macro Lett.* **2018**, *7*, 1364.
[7] D. Perera, L. Li, C. Walsh, J. Silliman, Y. Xiong, Q. Wang, H. C. Schniepp, *Acta Biomater.* **2023**, *168*, 323.
[8] D. Perera, Q. Wang, H. C. Schniepp, *Small* **2022**, *18*, 2202065.
[9] Q. Wang, P. McArdle, S. L. Wang, R. L. Wilmington, Z. Xing, A. Greenwood, M. L. Cotten, M. M. Qazilbash, H. C. Schniepp, *Nat. Commun.* **2022**,*13*, 4329.
[10] A. Sponner, E. Unger, F. Grosse, K. Weisshart, *Nat. Mater.* **2005**, *4*, 772.
[11] A. Sponner, W. Vater, S. Monajembashi, E. Unger, F. Grosse, K. Weisshart, *PLoS One* **2007**, *2*, e998.
[12] F. Vollrath, T. Holtet, H. C. Thogersen, S. Frische, *Proc. Biol. Sci.* **1996**, *263*, 147.
[13] J. B. Addison, T. M. Osborn Popp, W. S. Weber, J. S. Edgerly, G. P. Holland, J. L. Yarger, *RSC Adv.* **2014**, *4*, 41301.
[14] S. Okada, S. Weisman, H. E. Trueman, S. T. Mudie, V. S. Haritos, T. D. Sutherland, *Int. J. Biol. Macromol.* **2008**, *43*, 271.
[15] T. M. O. Popp, J. B. Addison, J. S. Jordan, V. G. Damle, K. Rykaczewski, S. L. Y. Chang, G. Y. Stokes, J. S. Edgerly, J. L. Yarger, *Langmuir* **2016**, *42*, 4681.
[16] S. D. Hudson, V. Zhurov, V. Grbic, M. Grbic, J. L. Hutter, *J. Appl. Phys.* **2013**, *113*, 154307.
[17] H. C. Schniepp, S. R. Koebley, F. Vollrath, *Adv. Mater.* **2013**, *25*, 7028.
[18] J. A. Coddington, H. D. Chanzy, C. L. Jackson, G. Raty, K. H. Gardner, *Biomacromolecules* **2001**, *3*, 5.
[19] D. P. Knight, F. Vollrath, *Philos. Trans. R. Soc. London Ser. B* **2002**, *357*, 219.
[20] J. A. Coddington, H. W. Levi, *Annu. Rev. Ecol. Syst.* **1991**, *22*, 565.
[21] C. E. Griswold, J. A. Coddington, N. I. Platnick, R. R. Forster, *J. Arachnol.* **1999**, *27*, 53.
[22] W. Eberhard, F. Pereira, *J. Arachnol.* **1993**, *21*, 161.
[23] R. F. Foelix, *Biology of Spiders*, Oxford University Press, USA **2011**.
[24] W. G. Eberhard, *Bull. Br. Arachnol. Soc.* **1988**, *7*, 247.
[25] A. C. Joel, P. Kappel, H. Adamova, W. Baumgartner, I. Scholz, *Arthropod Struct. Dev.* **2015**, *44*, 568.
[26] F. Vollrath, E. K. Tillinghast, *Naturwissenschaften* **1991**, *78*, 557.
[27] A. C. Hawthorn, B. D. Opell, *J. Exp. Biol.* **2003**, *206*, 3905.
[28] A. C. Hawthorn, B. D. Opell, *Biol. J. Linn. Soc.* **2002**, *77*, 1.
[29] N. I. Platnick, J. A. Coddington, R. R. Forster, C. E. Griswold, *Am. Mus. Novit.* **1991**, *1*, 3016.
[30] V. Friedrich, R. Langer, *Am. Zool.* **1969**, *9*, 91.
[31] H. M. Peters, *Ecophysiology of Spiders*, Springer, Berlin **1987**, p. 187.
[32] C. E. Griswold, M. J. Ramırez, J. A. Coddington, N. I. Platnick, in *Proceedings of the California Academy of Sciences 4th Series*, Vol. *56* (Eds: A. Leviton, G. C. Williams, M. L. Aldrich), California Academy of Sciences, California, USA **2005**, Supp. 2.
[33] A. C. Joel, A. Rawal, Y. Yao, A. Jenner, N. Ariotti, M. Weissbach, L. Adler, J. Stafstrom, S. J. Blamires, *Biomater. Sci.* **2023**, *11*, 2139.
[34] S. Stadlmayr, K. Peter, F. Millesi, A. Rad, S. Wolf, S. Mero, M. Zehl, A. Mentler, C. Gusenbauer, J. Konnerth, H. C. Schniepp, H. Lichtenegger, A. Naghilou, C. Radtke, *Adv. Healthcare Mater.* **2024**, *13*, 2302968.

[35] K. J. Koski, P. Akhenblit, K. McKiernan, J. L. Yarger, *Nat. Mater.* **2013**, *12*, 262.
[36] B. R. Neugirg, S. R. Koebley, H. C. Schniepp, *A. Fery Nanoscale* **2016**, *8*, 8414.
[37] T. W. Tombler, C. Zhou, L. Alexseyev, J. Kong, H. Dai, L. Liu, C. S. Jayanthi, M. Tang, S.-Y. Wu, *Nature* **2000**, *405*, 769.
[38] Q. Cheng, S. Wang, *Composites Part A* **2008**, *39*, 1838.
[39] M. Hudspeth, X. Nie, W. Chen, R. Lewis, *Biomacromolecules* **2012**, *13*, 2240.
[40] S. Santos, V. Barcons, H. K. Christenson, J. Font, N. H. Thomson, *PLoS One* **2011**, *6*, e23821.
[41] M. A. Collin, E. Camama, B. O. Swanson, J. S. Edgerly, C. Y. Hayashi, *Biomacromolecules* **2009**, *10*, 2268.
[42] I. Greving, M. Cai, F. Vollrath, H. C. Schniepp, *Biomacromolecules* **2012**, *13*, 676.
[43] S. R. Koebley, D. Thorpe, P. Pang, P. Chrisochoides, I. Greving, F. Vollrath, H. C. Schniepp, *Biomacromolecules* **2015**, *16*, 2796. .
[44] C. Holland, J. Urbach, D. Blair, *Soft Matter* **2012**, *8*, 2590.
[45] J. M. Gosline, P. A. Guerette, C. S. Ortlepp, K. N. Savage, *J. Exp. Biol.* **1999**, *202*, 3295.
[46] R. D. Jones, F. Di Gioacchino, H. Lim, T. E. J. Edwards, C. Schwalbe, C. C. Battaile, W. J. Clegg, *Sci. Rep.* **2018**, *8*, 8698.
[47] E. P. Debenedictis, S. Keten, *Soft Matter* **2019**, *15*, 1243.
[48] L. Römer, T. Scheibel, *Prion* **2008**, *2*, 154.
[49] J. Silliman, S. R. Koebley, H. C. Schniepp, *Harvard Dataverse* V1, https://doi.org/10.7910/DVN/Q05QVG.